An Analysis of WiFi Cochannel Interference at LTE Subcarriers and Its Application for Sensing

Prasanth Karunakaran(✉) and Wolfgang Gerstacker

Institute for Digital Communications, Friedrich-Alexander Universität Erlangen-Nürnberg, Erlangen 91058, Germany
{prasanth.karunakaran,wolfgang.gerstacker}@fau.de

Abstract. LTE-Unlicensed (LTE-U) involving the deployment of LTE in unlicensed bands has been gaining significant interest lately. The standardization of LTE-U has been proposed for Release 13 of 3GPP LTE. The two main requirements mandated for such an operation are the coexistence mechanisms with the WiFi systems and the sensing before transmission by an LTE-U device. Often in literature the interference in the LTE-U scenario is modeled as white Gaussian noise. There is a need to understand the properties of interference in such scenarios more accurately by taking into account the physical layer specifications of the LTE and the WiFi standards. To this end, we analyze the interference generated by a WiFi transmitter at an LTE receiver and characterize its correlation properties. We show that the interference powers across the LTE subcarriers exhibit a periodic behavior and that this can be exploited to develop sensing schemes selective to WiFi signals.

Keywords: LTE-U · WiFi · Interference · Statistics · Sensing · LBT

1 Introduction

The deployment of LTE systems [1] in the unlicensed spectrum, referred to as LTE-Unlicensed (LTE-U), has been gaining interest recently [2,3]. Even though an unlicensed spectrum is less reliable than a licensed spectrum, the LTE base stations (BSs) with carrier aggregation (CA) capabilities can potentially exploit the unlicensed spectrum to their advantage, improving their data rates [2]. Another possibility of interest is to consider LTE small cells as an alternative to WiFi small cells as illustrated in Fig. 1. One of the major issues in this context is the coexistence with other systems operating in the unlicensed band such as WiFi [2–9]. LTE, being developed originally for the licensed spectrum, lacks the required coexistence mechanisms for the unlicensed band. Due to these reasons, researchers from academia as well as industry have been studying this problem recently. Introducing a duty cycle in the LTE transmission is often considered as a suitable modification for enabling coexistence with the WiFi systems. In the throughput analysis of an LTE system for such situations, the WiFi interference when present is often treated as white noise [4–6]. However, it has been pointed

D. Noguet et al. (Eds.): CROWNCOM 2016, LNICST 172, pp. 605–617, 2016.
DOI: 10.1007/978-3-319-40352-6_50

out that the WiFi and the LTE systems have different physical layer characteristics and there is a need to study the impact of these differences [7] which we attempt to address in this work.

Most of the common WiFi standards such as 802.11a, 802.11n, 802.11ac etc. use an orthogonal frequency division multiplexing (OFDM) transmission with a subcarrier spacing of 312.5 kHz whereas the subcarrier spacing in LTE is 15 kHz. In the first part of this work, we analyze the properties of the co-channel interference generated by an OFDM WiFi transmitter at an LTE device. Starting from the continuous-time formulation of a WiFi signal, we derive the expression for the resulting co-channel interference due to the WiFi signal at the LTE subcarriers under a multipath propagation channel. Furthermore, the cross-correlation properties of the interference at the different subcarriers are derived and the accuracy of the analysis has been confirmed through simulations. Since the LTE subcarriers are significantly narrower than the WiFi subcarriers, the correlators corresponding to the subcarriers in an LTE receiver essentially perform a spectral analysis fine enough to measure the spectrum between the WiFi subcarriers. Each subcarrier in WiFi has a Sinc shaped spectrum which causes the power spectral density (PSD) of a WiFi signal to fall and rise from one WiFi subcarrier to the other. Because an LTE receiver is able to observe these variations, the WiFi interference power decreases and increases across the LTE subcarriers with a period corresponding to the WiFi subcarrier spacing. It is also shown that the magnitudes of the off-diagonal elements in the covariance matrix of the WiFi interference contributions at the different subcarriers are significantly smaller than that of the diagonal elements in the covariance matrix. We also provide a brief discussion of some of the implications for an LTE system.

Another requirement for LTE-U is the inclusion of sensing before transmission (SBT), also known as listen before talk (LBT) [2,8,9], to check the availability of a channel. The regulations governing the operation in the unlicensed spectrum in certain countries make this feature mandatory. The sensing functionality may be introduced at both the LTE transmitters and the receivers. Since multiple devices may be present within an LTE small cell, enabling the sensing at the devices can help to overcome the hidden node problem as illustrated in Fig. 1, where the LTE transmitter's sensing is rendered ineffective by

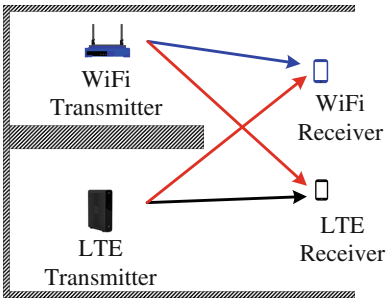

Fig. 1. WiFi-LTE interference scenario.

the blocking wall. Numerous algorithms for SBT have been developed in the context of cognitive radio (CR) systems such as energy detection (ED), cyclostationarity detection (CD) etc. [10]. Among them, ED has the least complexity. However, its operating point on the receiver operating characteristic (ROC) is highly sensitive to noise variance estimation errors. Algorithms based on CD are more complex but they do not require the knowledge of the noise variance making them constant false alarm detectors (CFADs). Though these algorithms may be useful, our interest is to find CFADs that can be easily incorporated into LTE devices. Therefore, in the second part of this work, we propose a sensing technique for WiFi signals, namely autocorrelation feature detection (AFD), that makes use of the periodic variation of the WiFi signal power across the LTE subcarriers and does not require the knowledge of the noise variance. This scheme can be easily implemented in LTE devices because it utilizes the signals received at the LTE subcarriers. The signal powers across the subcarriers can be interpreted as a PSD. As the PSD and the autocorrelation function (ACF) are Fourier transform pairs, the periodic fluctuations in the PSD indicate strong peaks in the ACF. The period of these fluctuations is equal to the WiFi subcarrier spacing (312.5 kHz) and the corresponding peaks in the ACF occur at $\pm\frac{1}{312.5\,\mathrm{kHz}} = \pm 3.2\mu\mathrm{s}$. Since this location is determined by the subcarrier spacing of the WiFi system, it is unlikely that signals other than a WiFi signal generate significant contributions at the feature position. In addition, we also obtain an approximate analytical expression for the false alarm probability of the AFD. It turns out that the analytical result agrees well with the false alarm probability achieved in the simulations. Our results show that the detector achieves a good detection performance even at low signal-to-noise ratios (SNRs) and that AFD can successfully distinguish a WiFi signal from an LTE signal. Furthermore, provided that the signal is contained in the sensing bandwidth, the AFD's performance is not affected by frequency offsets. Even for a low sensing bandwidth, the algorithm yields a decent performance which might turn out to be useful for LTE-M devices with low bandwidths designed for machine-type communications [13]. Excluding the OFDM discrete Fourier transform, which already is implemented in LTE devices, the complexity of this method is comparable to that of a time-domain ED with the same sensing duration.

The paper is organized as follows. Section 2 describes the system model and provides an analysis of the WiFi signal at the LTE subcarriers. In Sect. 3, the problem of SBT is introduced, the AFD is developed and its performance is evaluated via simulations. Section 4 concludes the paper.

2 System Model

The continuous-time signal transmitted by a single antenna WiFi transmitter can be written as

$$s(t) = \sqrt{P} \sum_{k\in\mathcal{F}} \sum_{l=-\infty}^{\infty} a_{k,l}\,\mathrm{rect}\left(\frac{t + T_{cp} - lT}{T}\right) \mathrm{e}^{j2\pi f_k (t-lT)}, \tag{1}$$

where $a_{k,l}$ is the zero mean transmit symbol with unit variance at subcarrier k of frequency f_k, which is an integer multiple of the subcarrier width Δf, and OFDM symbol l. $\mathcal{F}$ is the set of active WiFi subcarrier indices, $\mathrm{rect}(\frac{t}{T})$ represents a rectangular pulse with an amplitude of 1 situated at the interval $[0, T]$, $T_u = \Delta f^{-1}$ denotes the duration of the useful part of the OFDM symbol, T_{cp} stands for the duration of the cyclic prefix (CP) used in WiFi, and $T = T_u + T_{cp}$ is the duration of an OFDM symbol in WiFi. P refers to the transmit power per subcarrier. For typical WiFi systems, the values of these parameters are $T_u = 3.2\,\mu\mathrm{s}$, $\Delta f = 312.5\,\mathrm{kHz}$, $T_{cp} = 0.8\,\mu\mathrm{s}$ and $T = 4.0\,\mu\mathrm{s}$. For an M_τ-tap discrete multipath channel with the weight function $h(t,\tau) = \sum_{m=0}^{M_\tau - 1} h_m(t)\delta(\tau - \tau_m)$ ($h_m(t)$: channel coefficient of the mth path at time t, τ_m: delay of the mth path, M_τ: number of paths), the received signal contribution from the WiFi signal can be expressed as

$$r(t) = \int_{-\infty}^{\infty} s(t-\tau)h(t,\tau)\mathrm{d}\tau \tag{2}$$

$$= \sqrt{P}\sum_{k\in\mathcal{F}}\sum_{m=0}^{M_\tau-1}\phi_{mk}\sum_{l=-\infty}^{\infty} h_m(lT)a_{k,l}\theta_{kl}\mathrm{rect}\left(\frac{t-\tau_m+T_{cp}-lT}{T}\right)\mathrm{e}^{j2\pi f_k t}, \tag{3}$$

where $\phi_{mk} = \exp(-j2\pi f_k \tau_m)$ and $\theta_{kl} = \exp(-j2\pi f_k lT)$. Here, we assume that $h_m(t)$ remains constant within symbol intervals $[lT, (l+1)T], \forall l$. The contribution from $r(t)$ at a given subcarrier of frequency ν_i of an LTE receiver for the pth OFDM symbol, g_{ip}, can be obtained as follows

$$g_{ip} = \frac{1}{T_{u1}}\int_{pT_1}^{pT_1+T_{u1}} r(t)\mathrm{e}^{-j2\pi\nu_i t}\mathrm{d}t \tag{4}$$

$$= \frac{\sqrt{P}}{T_{u1}}\sum_{k\in\mathcal{F}}\sum_{m=0}^{M_\tau-1}\phi_{mk}\sum_{l=-\infty}^{\infty} h_m(lT)a_{k,l}\theta_{kl} \times\int_{pT_1}^{pT_1+T_{u1}}\mathrm{rect}\left(\frac{t-\tau_m+T_{cp}-lT}{T}\right)\mathrm{e}^{j2\pi(f_k-\nu_i)t}\mathrm{d}t \tag{5}$$

$$= \frac{\sqrt{P}}{T_{u1}}\sum_{m=0}^{M_\tau-1}\sum_{k\in\mathcal{F}}\sum_{l\in\mathcal{L}(p,\tau_m)}\phi_{mk}h_m(pT_1)a_{k,l}\theta_{kl}\underbrace{\int_{t_e(l,\tau_m,p)}^{t_n(l,\tau_m,p)}\mathrm{e}^{j2\pi(f_k-\nu_i)t}\mathrm{d}t}_{\beta_{ki}(l,\tau_m,p)}, \tag{6}$$

where $T_{u1} \approx 66.7\,\mu\mathrm{s}$ is the duration of the useful part of an LTE OFDM symbol which is equal to the reciprocal of the subcarrier width in LTE $\Delta f_1 = 15\,\mathrm{kHz}$, $T_1 \approx 71.4\,\mu\mathrm{s}$ represents the duration of an LTE OFDM symbol including its CP, and $\mathcal{L}(p,\tau_m)$ is the set of symbols which fall within the integration interval. $t_e(l,\tau_m,p)$ and $t_n(l,\tau_m,p)$ are the earliest and the latest time positions, respectively, of the lth WiFi symbol received over the mth path if this contribution lies in the integration interval of the pth LTE symbol. Here, we have also assumed

that the channel remains constant within an LTE symbol interval. $\beta_{ki}(l, \tau_m, p)$ can be simplified as follows

$$\beta_{ki}(l, \tau_m, p) = \begin{cases} t_n(l, \tau_m, p) - t_e(l, \tau_m, p), & \text{if } f_k = \nu_i, \\ \frac{e^{j2\pi(f_k-\nu_i)t_n(l)} - e^{j2\pi(f_k-\nu_i)t_e(l)}}{j2\pi(f_k-\nu_i)}, & \text{otherwise.} \end{cases} \tag{7}$$

Now, assuming uncorrelated transmit symbols and uncorrelated path gains, the correlation between the WiFi interference at subcarriers i and $i-o$ for the pth LTE symbol can be calculated as

$$r_{f,p}(i, o) = \mathbb{E}[g_{ip} g^*_{(i-o)p}] = \frac{P}{T^2_{u1}} \sum_{m=0}^{M_\tau - 1} P_m \sum_{k \in \mathcal{F}} \sum_{l \in \mathcal{L}(p, \tau_m)} \beta_{ki}(l, \tau_m, p) \beta^*_{k(i-o)}(l, \tau_m, p), \tag{8}$$

where $P_m = \mathbb{E}[|h_m(pT_1)|^2]$, assuming weak-sense stationary channel coefficients. For typical channels with maximum excess delay less than the cyclic prefix length used in LTE systems, the time correlation $r_{t,i}(p, o) = \mathbb{E}[g_{ip} g^*_{i(p-o)}]$ is zero for $|o| > 1$ as the contributing symbols are uncorrelated. As g_{ip} and $g_{i(p\pm1)}$ may share the same OFDM symbol at the integration boundaries, $r_{t,i}(p, o)$ may be non-zero for $|o| = 1$. However, this effect can be considered to be weak as the number of unshared symbols is about 15. It is also of interest to compute the correlation between interference at different subcarriers for a given channel state $\mathbf{h} = [h_0(pT_1), \cdots, h_{M_\tau - 1}(pT_1), \tau_0, \cdots, \tau_{M_\tau - 1}]^T$, denoted as $r_{f,p}(i, o, \mathbf{h})$. This parameter is of relevance to channel coding/decoding, link adaptation etc. which are performed over short intervals over which the channel is essentially static, and can be expressed as follows

$$\begin{aligned} r_{f,p}(i, o, \mathbf{h}) &= \mathbb{E}[g_{ip} g^*_{(i-o)p} | \mathbf{h}], \\ &= \frac{P}{T^2_{u1}} \sum_{k \in \mathcal{F}} \sum_{m=0}^{M_\tau - 1} \sum_{n=0}^{M_\tau - 1} h_m(pT_1) h^*_n(pT_1) \phi_{mk} \phi^*_{nk} \qquad (9) \\ &\quad \times \sum_{l \in \mathcal{L}(p, \tau_m) \cap \mathcal{L}(p, \tau_n)} \beta_{ki}(l, \tau_m, p) \beta^*_{k(i-o)}(l, \tau_n, p). \qquad (10) \end{aligned}$$

Simulations have been performed in order to confirm the anaytical results. In our simulations, random 16-QAM symbols have been selected as transmit symbols. The WiFi subcarrier frequencies used are $\Delta f \times [-26, \cdots, -1, 1, \cdots, 26]$ and an oversampling of 8 times the sampling rate of a 20 MHz LTE receiver is used to avoid aliasing effects. The analytical and simulation results for the correlations are presented in Figs. 2 and 3 which shows $r_{f,p}(i, 0)$ and $r_{f,p}(i, 0, \mathbf{h})$. The simulation results agree well with the analytical expressions. In both figures, it can be seen that the power fluctuates with a period of $\frac{\Delta f}{\Delta f_1} \approx 20$ subcarriers. This is because the magnitude of $\beta_{ki}(l, \tau_m, p)$ is inversely proportional to the

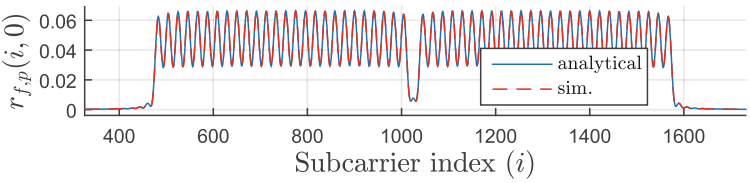

Fig. 2. Variance $r_{f,p}(i,0)$ of g_{i0} for a single tap channel with $P_0 = 1$.

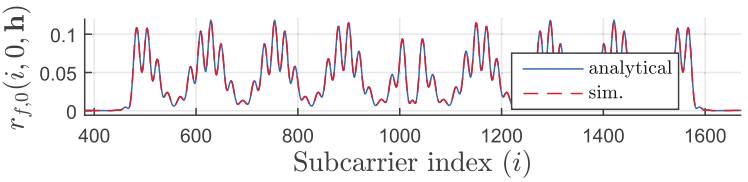

Fig. 3. Variance $r_{f,p}(i,0,\mathbf{h})$ of g_{i0} for a two tap channel with $h_0(t) = 1$, $h_1(t) = 0.5$, $\tau_0 = 0.0\,\mu s$ and $\tau_1 = 0.5\,\mu s$.

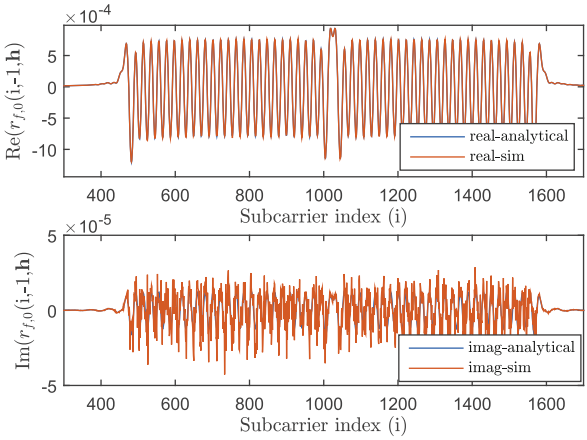

Fig. 4. Cross-correlation $r_{f,0}(i,-1,\mathbf{h})$ for a single path channel with $h_0(t) = 1$, $\tau_0 = 0.0\,\mu s$.

frequency separation $(f_k - \nu_i)$ and hence, the closer the LTE subcarrier is located to an active WiFi subcarrier the larger the power collected from it. Results for the cross-correlation $r_{f,0}(i,-1,\mathbf{h})$ at an offset of -1 are presented in Fig. 4. The analytical results again agree well with the simulations. It is interesting to note that the magnitude of the cross-correlation is significantly smaller than that of the variance in Fig. 3. These results indicate that the interference may be considered as uncorrelated across subcarriers. However, the significant difference in interference powers at different subcarriers must be taken into account in

performance evaluations when WiFi interference is assumed to be present. The knowledge of these power variations may be exploited to improve the channel estimation, channel quality computation, resource allocation etc. when a WiFi signal is interfering at an LTE receiver. Furthermore, since the periodic power variation is a characteristic of an LTE system with WiFi interference, such a fluctuation may be interpreted as a particular feature of a WiFi signal and can be used to distinguish between a WiFi signal and a non-WiFi signal in sensing, which is further explored in the next section.

3 WiFi Signal Sensing

The sensing before transmission in case of a WiFi signal potentially beginning at $t = 0$ by an LTE device is equivalent to a binary hypothesis testing problem given by

$$\begin{aligned} H_0 &: \ y_{ip} = n_{ip};\ i = 1, 2, \cdots, N;\ p = 0, 1, \cdots, M-1, \\ H_1 &: \ y_{ip} = g_{ip} + n_{ip};\ i = 1, 2, \cdots, N;\ p = 0, 1, \cdots, M-1, \end{aligned} \tag{11}$$

where H_1 and H_0 denote the hypotheses where a WiFi transmitter is active and inactive, respectively. y_{ip} is the received sample at the ith subcarrier of the pth OFDM symbol, n_{ip} denotes the circularly symmetric additive white Gaussian noise (AWGN) at the receiver ($n_{ip} \sim \mathcal{CN}(0, \sigma_n^2)$, σ_n^2 : noise variance) and g_{ip} represents the WiFi signal contribution defined according to (4). The noise is assumed to be independent and identically distributed (i.i.d.) over the subcarriers as well as the OFDM symbols with a variance given by $\sigma_n^2 = \frac{N_{0,PSD}}{T_{u1}}$ where $N_{0,PSD}$ is the noise power spectral density. N and M stand for the maximum number of subcarriers (LTE DFT size) and the number of LTE OFDM symbols used in the sensing process, respectively. We restrict our attention to sensing schemes that can be implemented in the LTE subcarrier domain and also without the knowledge of the noise variance, thereby making them suitable for existing LTE receivers.

3.1 Autocorrelation Feature Detection (AFD)

In this approach, we make use of the periodic fluctuations of the variance of g_{ip} ($i = N_0, \cdots, N_1$) resulting from the difference in subcarrier widths of LTE and WiFi systems as illustrated in Figs. 2 and 3. N_0 and N_1 are adjusted to select the bandwidth used in sensing. The number of subcarriers used for sensing is $N_{tot} = N_1 - N_0 + 1$ ($1 \leq N_0 < N_1 \leq N$). According to the LTE standard, a 20 MHz receiver uses $N = 2048$ and its sampling frequency is $N\Delta f_1 = 30.72$ MHz. For this receiver, setting $N_0 = 1$ and $N_1 = N$ selects the whole 30.72 MHz bandwidth for the sensing process. The time average of the powers at the different subcarriers can be interpreted as an estimate of the power spectral density of a WiFi signal after passing through the correlators corresponding to the LTE subcarriers. Periodic fluctuations in the power spectral density indicate a strong peak in its DFT coefficient sequence, which can

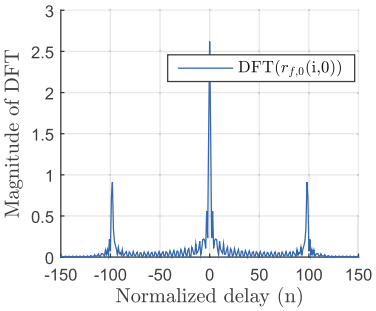

Fig. 5. Magnitude of DFT of the sequence in Fig. 2.

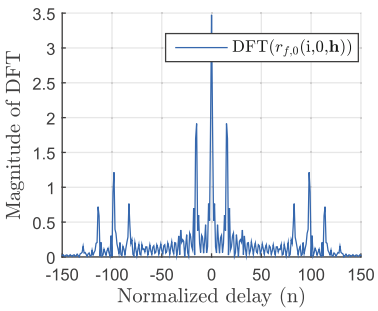

Fig. 6. Magnitude of DFT of the sequence in Fig. 3.

be interpreted as the complex conjugate of an autocorrelation function. If the averaging is performed over a duration smaller than the coherence time of the channel, additional peaks may be present whose locations depend on the path delays. The channel independent peaks in the N_{tot}-point DFT of the vector $\mathbf{r}_{f,p}(0) = [r_{f,p}(N_0, 0), \cdots, r_{f,p}(N_1, 0)]^T$ are fixed by the subcarrier widths and located at the integer closest to $\frac{\pm N_{tot}\Delta f_1}{\Delta f}$. They can be considered as a particular feature corresponding to a WiFi signal.

For $N_{tot} = 2048$ ($N_0 = 1$, $N_1 = 2048$), the peaks occur at the normalized delays ± 98 (i.e., $\pm 3.2\,\mu$s). This is illustrated in Figs. 5 and 6 where the magnitudes of the autocorrelation function computed from the 2048-point DFT of the sequences $r_{f,p}(i, 0)$ (long-term averaging) and $r_{f,p}(i, 0, \mathbf{h})$ (short-term averaging) are shown. The additional peaks in Fig. 6 are due to the static two path channel. The results imply that when a channel delay exists at $3.2\,\mu$s, and the averaging length is short, this peak is spurious for the detection of WiFi signals. However, since the maximum delays encountered in indoor small cells environments are typically much smaller than $3.2\,\mu$s [11], we can safely assume that the peaks at $\pm 3.2\,\mu$s are from a WiFi signal. To develop a detector exploiting this feature, we define $r_i = \frac{1}{M}\sum_{p=1}^{M} |y_{ip}|^2$, $\mathbf{r}_y = [r_{N_0}, \cdots, r_{N_1}]^T$ and $\mathbf{v}_y = \mathbf{F}\mathbf{r}_y$, where $\mathbf{F}$ is the unitary N_{tot}-point DFT matrix. $\mathbf{r}_y$ is a vector of time averaged subcarrier powers and therefore, its DFT $\mathbf{v}_y$ is conjugate symmetric. Without loss of generality, we assume N_{tot} is even. Let $v_y(n)$ indicate the element of $\mathbf{v}_y$ corresponding to the normalized delay n. Then, our feature detector is expressed as follows

$$T_2 = \frac{|\mathcal{D}_1| \sum_{n\in\mathcal{D}_0} |v_y(n)|^2}{|\mathcal{D}_0| \sum_{n\in\mathcal{D}_1} |v_y(n)|^2} > t_2, \tag{12}$$

where $\mathcal{D}_0 = \{n_0\}$ (n_0: the positive normalized delay corresponding to the feature position), $\mathcal{D}_1 = \{1, \cdots, \frac{N_{tot}}{2} - 1\} \sim \mathcal{D}_0$ ($\sim$: set difference, $|\mathcal{D}_k|$: cardinality of $\mathcal{D}_k$) contains all the positive delays except n_0 and t_2 is the threshold for a desired false alarm probability which can be computed analytically. In the following, we assume that H_0 holds unless otherwise specified. In this case, r_i is the sum of the squared magnitudes of M i.i.d. complex Gaussian random variables. For

large M, using the central limit theorem, approximation $r_i \sim \mathcal{N}(a, b^2 - a^2)$ becomes accurate where $a = \mathbb{E}[r_i] = \sigma_n^2$ and $b^2 = \mathbb{E}[|r_i|^2] = \sigma_n^4(1 + \frac{1}{M})$. Also, for $i \neq j$, $\mathbb{E}[r_i r_j^*] = \mathbb{E}[r_i]\mathbb{E}[r_j^*] = \sigma_n^4$. Therefore, $\mathbf{r}_y \sim \mathcal{N}(\boldsymbol{\mu}_r, \mathbf{C}_r - \boldsymbol{\mu}_r \boldsymbol{\mu}_r^H)$, where $\boldsymbol{\mu}_r = \sigma_n^2 \mathbf{1}$ ($\mathbf{1}$:vector with all elements equal to one) and $\mathbf{C}_r$ is a circulant matrix whose first column is given by $\mathbf{c}_{r1} = \sigma_n^4 \mathbf{1} + [\frac{\sigma_n^4}{M}, 0, \cdots, 0]^T$. Now, $\mathbb{E}[\mathbf{v}_y] = \sigma_n^2 \mathbf{F1} = \sigma_n^2 [\sqrt{N_{tot}}, 0, \cdots, 0]^T$ and using the diagonalization property of circulant matrices, we obtain $\mathbb{E}[\mathbf{v}_y \mathbf{v}_y^H] = \mathbf{F}\mathbf{C}_r\mathbf{F}^H = \text{diag}(\sqrt{N_{tot}}\mathbf{F}\mathbf{c}_{r1}) = \sigma_n^4 \cdot \text{diag}(N_{tot} + \frac{1}{M}, \frac{1}{M}, \cdots, \frac{1}{M})$. This shows that the denominator of T_2 is the sum of squared magnitudes of $(\frac{N_{tot}}{2} - 2)$ i.i.d. complex Gaussian random variables which has a central Chi-squared distribution with $2(\frac{N_{tot}}{2} - 2)$ degrees of freedom [12], and the numerator is Chi-squared distributed with 2 degrees of freedom. Therefore, for large M, T_2 under H_0 follows a central F-distribution with 2 numerator degrees of freedom and $2(\frac{N_{tot}}{2} - 2)$ denominator degrees of freedom [12]. The threshold for a desired false alarm probability can be obtained using the corresponding tail probability function. Figure 7 shows the analytical and simulation results for the false alarm probability for $M = 20$ and $N_{tot} = 2048$. The results indicate that the approximations adopted provide a sufficient accuracy.

An interesting aspect of this method is that it is unaffected by frequency offsets that translate the WiFi spectrum to another part of the slice of subcarriers under inspection. This is because the magnitude of the DFT coefficients is not affected by translations. Furthermore, this method is quite insensitive to non-WiFi signals because it targets a WiFi specific feature. It can also be applied in LTE devices designed for bandwidths smaller than 20 MHz (for e.g., LTE-M [13]).

3.2 Autocorrelation Detection (AD)

If our interest is to detect the presence of any signal (not only WiFi), all the normalized delays where the signal is expected to have a significant contribution and the average autocorrelation contribution from noise is zero can be considered. This is accomplished by setting $\mathcal{D}_0 = \{1, \cdots, L_+\}$, where L_+ is chosen such that all the DFT coefficients where the contributions of the signals to be detected have appreciable strengths are included in $\mathcal{D}_0$. The threshold for a desired false

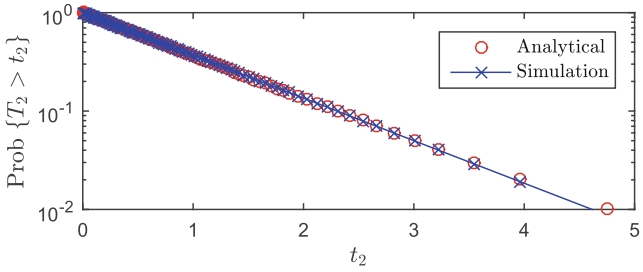

Fig. 7. Tail probability of T_2 for $M = 20$ and $N = 2048$.

alarm probability can be obtained by performing an analysis similar to the one used for the AFD.

3.3 Performance Comparison

Simulations have been conducted to compare the performance of the AD and the AFD. In indoor small cell scenarios, the user mobility is expected to be quite limited. For example, at a carrier frequency of 5.5 GHz and for a Jakes' Doppler power spectrum, the coherence time, defined as the time separation at which the magnitude of the time autocorrelation function of the channel becomes half of its peak value, for a speed of 7 km/hr is given by 6.7 ms which spans about 93 LTE OFDM symbols. Since the value of $M = 20$ used in the simulations is much smaller than 93, the channel is assumed to be quasi-static

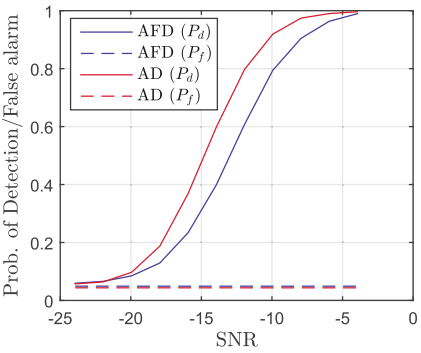

Fig. 8. WiFi signal sensing with $M = 20$ (1.4 ms) and $N_{tot} = 2048$ (Bandwidth = 30.72 MHz).

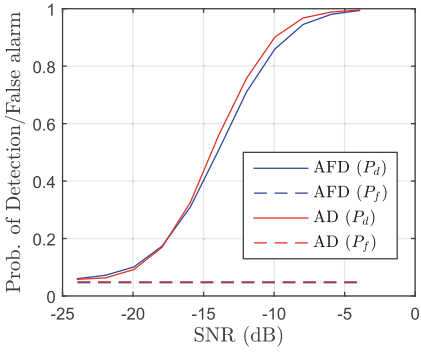

Fig. 9. WiFi signal sensing with $M = 20$ (1.4 ms), $N_{tot} = 1332$ (Bandwidth = 20 MHz) and a frequency offset of $150\Delta f_1$.

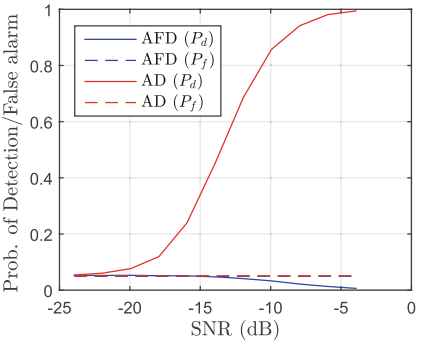

Fig. 10. LTE signal sensing with $M = 20$ (1.4 ms) and $N_{tot} = 1332$ (Bandwidth = 20 MHz).

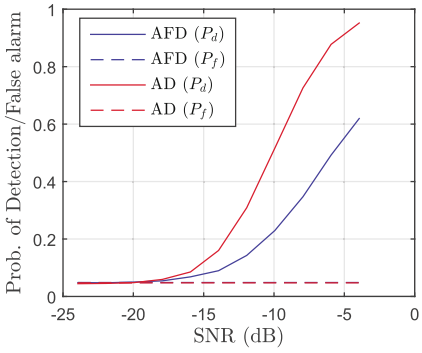

Fig. 11. WiFi signal sensing with $M = 20$ (1.4 ms) and $N_{tot} = 128$ (Bandwidth = 1.92 MHz).

over the sensing interval. However, this is not a requirement for the proposed algorithms. A three tap channel is used with the path delays located at $\tau_0 = 0$ μs, $\tau_1 = 1$ μs and $\tau_2 = 2$ μs, and relative powers of 0 dB, −3 dB and −6 dB, respectively. The number of channel realizations has been set to 10000. The noise PSD is calculated as $N_{0,PSD} = F_{rx} K_B T_k$ where $F_{rx} = 8$ dB is the receiver noise figure, $K_B = 1.38 \times 10^{-23}$ Ws/K is the Boltzmann's constant and $T_k = 293$ K is the room temperature. The WiFi signal generated in simulations occupies the central 52 subcarriers other than the DC subcarrier and the LTE signal generated corresponds to a 20 MHz signal where the central 1200 carriers excluding the DC carrier are loaded. Three subcarrier slices, corresponding to a spectral width of 30.72 MHz ($N_0 = 1, N_1 = 2048$), 20 MHz ($N_0 = 359, N_1 = 1690$) and 1.92 MHz ($N_0 = 961, N_1 = 1088$), are chosen to realize different sensing bandwidths. The SNR is always referred to the total signal power of the original 20 MHz WiFi signal and a receiver bandwidth of 30.72 MHz for which the noise power is −91 dBm. The total receive signal power is equally divided between the used subcarriers and is increased from −115 dBm to −95 dBm, changing the SNR from −24 dB to −4 dB. The desired false alarm probability is chosen as 0.05 and the analytical results are used to set the threshold for both the schemes. The simulation results for the probability of detection (P_d) and the probability of false alarm (P_f) are presented in Figs. 8, 9, 10 and 11. AD uses $L_+ = n_0 + 10$. The simulation results show that the achieved false alarm probability is quite close to the target value, confirming the accuracy of the analysis. AD outperforms AFD because the former collects the contribution from all significant taps including the feature. Figure 9 depicts the performance under a frequency offset of 150 LTE subcarrier spacings and demonstrates the immunity of the autocorrelation based methods to frequency offsets, as discussed in Sect. 3.1. For the very low sensing bandwidth case of Fig. 11, both the schemes suffer due to the reduction in number of samples. The impact on the AFD is more significant than on the AD. However, as shown Sect. 3.1, the noise contributions affecting the test statistic can be reduced by increasing M and the performance can be improved even for the low bandwidth cases. Therefore, this method is suitable for LTE devices with low system bandwidths which might turn out to be useful in LTE-M scenarios [13]. Finally, the detection performance of the algorithms for a 20 MHz system when an LTE signal is used instead of a WiFi signal is shown in Fig. 10. As expected, AD is also suitable for the LTE signal. AFD is not triggered because it targets a specific feature that results when a WiFi signal passes through an LTE receiver. Since the maximum channel delay used in the simulation is 2 μs, there is hardly any contribution from the LTE signal at the feature position. Due to the way T_2 is defined, the contribution of the LTE signal in the denominator of T_2 scales down the numerator term more heavily as the LTE signal strength is raised. As a result, when the signal power is increased, the PDF of T_2 under H_1 shifts to the left side compared to the PDF of T_2 under H_0 and the detection probability falls below the false alarm probability. This does not occur for a WiFi signal due to the strength of the feature position in the numerator of T_2. Regarding complexity of the proposed schemes, compared to a time-domain

energy detector the main increase in complexity stems from the additional DFT that is needed for each symbol. However, an LTE device already includes a DFT module as a part of its OFDM receiver. Besides, DFTs can be implemented efficiently via the fast Fourier transform.

4 Conclusions

In this work, we have analyzed the correlation properties of the interference introduced by a WiFi transmitter at an LTE receiver. It is shown that the interference powers across the LTE subcarriers from a WiFI system exhibit a periodic behavior. The knowledge of this behavior might turn out to be useful in the design of algorithms for LTE-U scenarios. Furthermore, it is demonstrated that the periodic variation of the interference can be exploited in sensing, even by low bandwidth LTE devices, to detect WiFi signals as well as to distinguish WiFi signals from other signals.

References

1. 3GPP TS 36.211: Evolved Universal Terrestrial Radio Access (E-UTRA): Physical Channels and Modulation. Version 12.1.0 (2014). http://www.3gpp.org/dynareport/36211.htm
2. QUALCOMM: Extending LTE Advanced to Unlicensed Spectrum. White paper (2014). http://www.qualcomm.com/media/documents/white-paper-extending-lte-advanced-unlicensed-spectrum
3. Abinader, F.M., et al.: Enabling the coexistence of LTE and Wi-Fi in unlicensed bands. IEEE Commun. Mag. **52**(11), 54–61 (2014)
4. Sagari, S., Seskar, I., Raychaudhuri, D.: Modeling the coexistence of LTE and WiFi heterogeneous networks in dense deployment scenarios. In: Proceedings of the IEEE International Conference on in Communication (ICC), pp. 2301–2306 (2015)
5. Bhorkar, A., Ibars, C., Zong, P.: On the throughput analysis of LTE and WiFi in unlicensed band. In: Proceedings of the 48th Asilomar Conference on in Signals, Systems and Computers, pp. 1309–1313 (2014)
6. Rupasinghe, N., Güvenc, İ.: Licensed-assisted access for WiFi-LTE coexistence in the unlicensed spectrum. In: Proceedings of the IEEE Globecom Workshops, pp. 894–899 (2014)
7. Zhang, R., Wang, M., Cai, L.X., Zheng, Z., Shen, X.: LTE-unlicensed: the future of spectrum aggregation for cellular networks. IEEE Wirel. Commun. **22**, 150–159 (2015)
8. Chen, C., Ratasuk, R., Ghosh, A.: Downlink performance analysis of LTE and WiFi coexistence in unlicensed bands with a simple listen-before-talk scheme. In: Proceedings of the 81st IEEE Vehicular Technology Conference (VTC Spring), pp. 1–5 (2015)
9. Bhorkar, A., Ibars, C., Papathanassiou, A., Zong, P.: Medium access design for LTE in unlicensed band. In: Proceedings of the IEEE Wireless Communications and Networking Conference (WCNC), pp. 369–373 (2015)
10. Yucek, T., Arslan, H.: A survey of spectrum sensing algorithms for cognitive radio applications. IEEE Commun. Surv. Tutorials **11**, 116–130 (2009)

11. Durgin, G., Kukshya, V., Rappaport, T.: Wideband measurements of angle and delay dispersion for outdoor and indoor peer-to-peer radio channels at 1920 MHz. IEEE Trans. Antennas Propag. **51**, 936–944 (2003)
12. Kay, S.M.: Fundamentals of Statistical Signal Processing: Detection Theory. Prentice Hall, New York (1998)
13. Nokia Networks: LTE-M - Optimizing LTE for the Internet of Things. White paper (2015). http://networks.nokia.com/innovation/futureworks-publications